Published in final edited form as:
Biomaterials. 2011 August ; 32(23): 5330–5340. doi:10.1016/j.biomaterials.2011.04.021.

The effect of anisotropic collagen-GAG scaffolds and growth factor supplementation on tendon cell recruitment, alignment, and metabolic activity

Steven R. Caliari[a] and **Brendan A.C. Harley**[a,b,*]

[a]Dept. Chemical and Biomolecular Engineering, University of Illinois at Urbana-Champaign, Urbana, IL 61801, USA

[b]Institute for Genomic Biology University of Illinois at Urbana-Champaign, Urbana, IL 61801, USA

Abstract

Current surgical and tissue engineering approaches for treating tendon injuries have shown limited success, suggesting the need for new biomaterial strategies. Here we describe the development of an anisotropic collagen-glycosaminoglycan (CG) scaffold and use of growth factor supplementation strategies to create a 3D platform for tendon tissue engineering. We fabricated cylindrical CG scaffolds with aligned tracks of ellipsoidal pores that mimic the native physiology of tendon by incorporating a directional solidification step into a conventional lyophilization strategy. By modifying the freezing temperature, we created a homologous series of aligned CG scaffolds with constant relative density and degree of anisotropy but a range of pore sizes (55–243 μm). Equine tendon cells showed greater levels of attachment, metabolic activity, and alignment as well as less cell-mediated scaffold contraction, when cultured in anisotropic scaffolds compared to an isotropic CG scaffold control. The anisotropic CG scaffolds also provided critical contact guidance cues for cell alignment. While tendon cells were randomly oriented in the isotropic control scaffold and the transverse (unaligned) plane of the anisotropic scaffolds, significant cell alignment was observed in the direction of the contact guidance cues in the longitudinal plane of the anisotropic scaffolds. Scaffold pore size was found to significantly influence tendon cell viability, proliferation, penetration into the scaffold, and metabolic activity in a manner predicted by cellular solids arguments. Finally, the addition of the growth factors PDGF-BB and IGF-1 to aligned CG scaffolds was found to enhance tendon cell motility, viability, and metabolic activity in dose-dependent manners. This work suggests a composite strategy for developing bioactive, 3D material systems for tendon tissue engineering.

Keywords

Collagen; Scaffold; Tendon; Growth factors; Porosity

1. Introduction

The extracellular matrix (ECM) is an elaborate macromolecular structure that defines the physical morphology of tissues and the local environment surrounding cells. In addition to serving as a physical support structure and insoluble regulator of cell activity, the ECM is a

*Corresponding author. Dept. of Chemical and Biomolecular Engineering, Institute of Genomic Biology, University of Illinois at Urbana-Champaign, 110 Roger Adams Laboratory, 600 S. Mathews Ave. Urbana, IL 61801. Tel.: +1 217 244 7112; fax: +1 217 333 5052. bharley@illinois.edu. .

reservoir for numerous soluble regulators of cell behavior. As analogs of the native ECM, collagen-glycosaminoglycan (CG) scaffolds have previously been used in a variety of soft tissue engineering applications, both *in vivo* as regenerative templates for skin, peripheral nerves, conjunctiva, and cartilage [1–3] as well as *in vitro* as model systems for studies of cell–matrix interactions [4,5]. These scaffolds possess a 3D structure with requisite porosity (>99%) and bioactivity for studies of tissue regeneration while also being regulatory compliant [6]. Recently, CG scaffolds have been developed for bone and osteochondral tissue engineering applications [7,8]. Here we seek to extend the utilization of CG scaffolds towards tendon tissue engineering.

Tendon is primarily composed of tendon cells (TCs) distributed within a hierarchical arrangement of type I collagen fibrils aligned along its tensile axis [9,10]. Tendon and ligament injuries, both acute and chronic, are exceedingly common, with over 32 million occurring each year in the US [9–12]. While small tendon injuries can heal via regeneration, larger tendon defects undergo a repair-mediated process resulting in the formation of fibrocartilagenous scar tissue. Most severe tendon injuries, in stark contrast to fetal wound healing processes which can regenerate damaged tissue [13], demonstrate an incomplete remodeling stage resulting in a poorly aligned ECM with inferior functional properties [9,10,12].

Improved strategies are needed to enable functional regeneration of severe tendon injuries. Ineffective repair of acute tendon injuries does not produce tissues that recapitulate the native physical properties of tendon, permanently precluding a return to normal function. Autograft and allograft procedures represent the current clinical gold-standard for treating tendon injuries [14], but are plagued by limited availability and stringent processing requirements for allograft tissue as well as secondary wound site creation and resultant loss of function for autografts. Biomaterial constructs such as tissue engineering scaffolds represent an important alternative, but significant optimization is still required. Tissue engineering scaffolds should ideally possess several key features including high porosity and permeability, three-dimensionality, ligands for cells to attach onto, mechanical competence, tunable degradation, and biocompatibility [10,15]. Due to mechanical concerns and the inherent ability to create highly anisotropic structures, many tendon tissue engineering materials are designed as woven or electrospun synthetic polymer mats instead of 3D scaffolds [10,16,17]. Electrospun synthetic biomaterials have demonstrated tensile elastic moduli approaching that of tendon along with some success in *in vivo* settings [10,17,18]. In order to develop more optimized variants of these materials, a variety of techniques have emerged to supplement construct bioactivity, namely providing contact guidance cues via the 2D surface topology as well as growth factor supplementation [9,10].

Scaffold-based systems offer the potential for aligned 3D microenvironments for tendon repair, but a number of structural, biomolecular, and mechanical features require optimization. For example, a range of studies have suggested that successful regeneration templates for natively aligned tissues such as peripheral nerves [19], the myocardium [20], and tendon [10,17,21,22] must provide tissue specific aligned contact guidance cues that recapitulate aspects of the tissue anisotropy. In addition to degree of anisotropy, which can also significantly influence scaffold modulus [23], CG scaffold pore size has been repeatedly shown to significantly impact scaffold bioactivity due to its opposing effects on specific surface area (increasing with decreasing pore size) and permeability (increasing with pore size) [24,25]. Cell confinement within anisotropic 3D structures may also significantly impact scaffold bioactivity. TCs cultured on corrugated 2D substrates demonstrated increased maintenance of tendon-like phenotype and gene expression as well as significant differences in TC orientation, proliferation, and collagen biosynthesis versus non-patterned controls; notably, the effect of contact guidance cues was strongly dependent

on the spacing between the corrugated substrate contact guidance cues [26,27]. Taken together, these results suggest that structurally anisotropic (aligned) CG scaffolds could significantly improve TC bioactivity and scaffold regenerative potential relative to an isotropic (non-aligned) variant, and that this effect may be co-dependent on pore size, which defines lateral spacing between contact guidance cues and influences local surface area and biomolecule diffusion.

Growth factor supplementation strategies have shown significant functional value in the context of tendon tissue regeneration [28–30]. Platelet-derived growth factor-BB (PDGF-BB) and insulin-like growth factor 1 (IGF-1) have been implicated as key factors in aiding the recruitment of TCs to the wound site during early wound healing [9,10]. Individually, PDGF-BB [29,31] and IGF-1 [32] have been shown to alter TC proliferation and collagen synthesis capacity in dose-dependent manners; synergistic effects of PDGF-BB and IGF-1 have also been noted [29–31]. PDGF-BB and IGF-1 have additionally been indicated to be activators of mesenchymal stem cell (MSC) chemotaxis [33–35], and most importantly from a regenerative standpoint have been shown to improve *in vivo* rotator cuff healing in a rat model [36].

This manuscript describes the development of a porous CG scaffold that integrates both insoluble (contact guidance via scaffold anisotropy) and soluble (growth factor) cues for tendon tissue engineering. The aligned microstructure and an optimized pore size were hypothesized to improve construct regenerative capacity by providing aligned contact guidance cues to TCs within the network. PDGF-BB and IGF-1 supplementation was further hypothesized to aid initial TC recruitment and subsequent proliferation within the originally acellular CG scaffold. While CG scaffolds have previously been integrated with gene delivery vehicles for *in vitro* meniscus and cartilage tissue engineering [37,38], the combined effect of growth factor supplementation within an anisotropic microstructure has not been explored for tendon tissue engineering.

2. Materials and methods

2.1. CG scaffold fabrication

CG scaffolds were fabricated via lyophilization from a suspension of type I microfibrillar collagen from bovine dermis (Devro Inc., Columbia, SC) and chondroitin sulfate derived from shark cartilage (Sigma–Aldrich, St. Louis, MO) in 0.05 M acetic acid [1,39,40]. Prior to lyophilization the suspension was maintained at 4 °C to prevent gelatinization. All scaffolds were fabricated in a Genesis freeze-dryer (VirTis, Gardiner, NY) from a constant CG suspension, resulting in scaffolds with distinct microstructural properties but a constant relative density (ρ^*/ρ_s, 0.006). Anisotropic CG scaffolds were fabricated by a directional solidification step using a custom polytetrafluoroethylene (PTFE) and copper mold prior to sublimation (0 °C, 200 mTorr). The mold consisted of a PTFE block with cylindrical wells (6 mm diameter, 15 mm deep) extending to a 1/16″ thick copper base plate. The CG suspension was pipetted into the PTFE-copper mold and placed onto a pre-cooled freeze-dryer shelf (−10, −40, or −60 °C) (Fig. 1(a)). The rapid solidification and significant thermal conductivity mismatch of the mold materials ($k_{Cu}/k_{PTFE} \sim 1600$) was hypothesized to promote unidirectional heat transfer through the copper bottom. The suspension was then held at the specified freezing temperature for > 1 h to ensure complete solidification. An isotropic control CG scaffold was fabricated using a previously developed constant cooling rate method so as to induce uniform solidification profiles throughout the suspension [41,42]. The CG suspension was placed in an aluminum tray mold into the freeze-dryer at a starting shelf temperature of 4°C and then frozen to a final freezing temperature of −40 °C. For all variants, ice crystals were then sublimated under vacuum (200 mTorr) at 0 °C to produce porous CG scaffolds.

Scaffolds were sterilized and dehydrothermally crosslinked at 105 °C for 24 h under vacuum (<25 torr) in a vacuum oven (Welch, Niles, IL). Scaffolds were then immersed in 100% ethanol overnight, washed with phosphate-buffered saline (PBS), and further crosslinked using carbodiimide chemistry in a solution of 1-ethyl-3-[3-dimethylaminopropyl] carbodiimide hydrochloride (EDAC) and *N*-hydroxysulfosuccinimide (NHS) at a molar ratio of 5:2:1 EDAC:NHS:COOH [43,44]. Scaffolds were then rinsed and stored in PBS until use.

2.2. SEM analysis

Scanning electron microscope (SEM) analysis was used to qualitatively assess scaffold microstructural organization (pore size, shape). SEM analysis was performed with a JEOL JSM-6060LV Low Vacuum Scanning Electron Microscope (JEOL USA, Peabody, MA) using both a secondary electron (SE) detector and a backscatter electron (BSE) detector under low vacuum (variable pressure) mode, allowing scaffolds to be visualized without a conductive coating [7].

2.3. Quantitative microstructural analysis

The cylindrical CG scaffolds (15 mm length) were cut into three 5 mm sections: bottom (closest to freeze-dryer shelf), middle, and top. Each section was embedded in glycolmethacrylate and longitudinal and transverse scaffold sections (5 μm thick) were serially cut on a microtome and stained with aniline blue to allow visualization of the CG strut network in a manner previously described [41]. Images were acquired at 10× magnification on an optical microscope (Leica Microsystems, Germany) and analyzed using a linear intercept macro in Scion Image. The program calculated a best-fit ellipse representation of the average pore in each histology section and gave fitting parameters to determine pore size and aspect ratio (AR), the ratio of the major and minor axes of the best-fit ellipse [41].

2.4. Cell culture

2.4.1. Tendon cell isolation and expansion—Primary TCs were harvested fresh from horses 2–3 years in age euthanized for reasons not related to tendinopathy in a manner approved by the University of Illinois IACUC. Digital flexor tendons were removed, diced, incubated in collagenase for 24 h under agitation, and strained through a 40 μm filter, to isolate TCs [27]. TCs were cultured in standard culture flasks in high glucose Dulbecco's modified Eagle's medium (DMEM, Fisher, Pittsburgh, PA) supplemented with 10% fetal bovine serum (FBS, Invitrogen, Carlsbad, CA), 1% L-glutamine (Invitrogen, Carlsbad, CA), 1% penicillin/streptomycin (Invitrogen, Carlsbad, CA), 1% amphotericin-B (MP Biomedical, Solon, OH), and 25 μg/mL ascorbic acid (Wako, Richmond, VA) [27]. Cells were fed every 3 days and cultured to confluence at 37 °C and 5% CO_2. Passage 2 or 3 TCs were used throughout.

2.4.2. Scaffold culture conditions—CG scaffold plugs (6 mm diameter, ~5 mm thickness) were cut from the middle section of full length scaffolds and were placed in ultra-low attachment 6-well plates (Corning Life Sciences, Lowell, MA) and seeded with TCs using a previously validated method [45]. Confluent TCs were trypsinized and resuspended at a concentration of 5×10^5 cells per 20 μL media. 10 μL of cell suspension (2.5×10^5 cells) was added to each scaffold. The scaffolds were then incubated at 37 °C for 15 min, turned over, and seeded with an additional 10 μL of cell suspension for a total of 5×10^5 cells seeded per scaffold. Scaffolds were incubated at 37 °C and 5% CO_2 and fed with complete DMEM every 3 days for the duration of all experiments. For experiments involving soluble factor supplementation, scaffolds were cultured in serum-free DMEM to eliminate the influence of exogenous serum components. Human recombinant (rh) PDGF-

BB and IGF-1 were purchased from R&D Systems (Minneapolis, MN) and reconstituted in the manufacturer's recommended solutions. Soluble factors were diluted to proper concentrations in serum-free media for culture experiments. Soluble factor supplemented, serum-free media was changed every 3 days.

2.5. Tendon cell chemotaxis assay

The ability of TC chemotaxis mechanisms to improve the speed of cellular penetration into aligned CG scaffold constructs was tested with a modified Transwell membrane experiment. CG scaffolds were placed in 24-well plates below conventional polycarbonate Transwell membrane inserts (8 μm pore size, 6.5 mm diameter; Fisher Scientific, Pittsburgh, PA). Scaffolds were cut to size so that they were in direct contact with the membrane above without being compressed. Serum-free DMEM supplemented with a range of therapeutic doses of PDGF-BB (10, 50, 100 ng/ml) and IGF-1 (50, 100, 500 ng/ml) was placed in the lower chamber with the CG scaffold; 5×10^5 TCs were added to the top side of the Transwell membrane in serum-free, non-supplemented DMEM. Controls with supplemented media in both chambers were performed to assess TC chemokinesis versus chemotaxis in response to PDGF-BB supplementation. After 24 h, the number and metabolic activity of the cells that had migrated into the scaffold was determined.

2.6. Determination of cell number

The total number of cells attached to each scaffold was determined via DNA quantification. Scaffolds were washed in PBS to remove unattached and dead cells and then placed in a papain solution at 60 °C for 24 h to both digest the scaffold and lyse the cells to expose their DNA. A Hoechst 33258 dye (Invitrogen, Carlsbad, CA) was used to fluorescently label double-stranded DNA [46] and assayed via a fluorescent spectrophotometer (Varian, Santa Clara, CA). Experimental readings were compared to a standard curve created by measuring the fluorescence levels for a range of known cell numbers to calculate cell attachment as a percentage of the total number of seeded cells [46].

2.7. Determination of cell metabolic activity

The metabolic activity of the cells within each scaffold was determined by a nondestructive alamarBlue assay. Viable cells continuously convert the active ingredient in alamarBlue (resazurin) to a fluorescent byproduct (resorufin), allowing comparison of the gross metabolic activity of each cell-seeded construct. Cell-seeded scaffolds were incubated at 37 °C in 1x alamarBlue (Invitrogen, Carlsbad, CA) solution with gentle shaking for 3 h [47]. Resorufin fluorescence was determined via a fluorescent spectrophotometer (Varian, Santa Clara, CA). Relative cell metabolic activity was determined and reported as a percentage of the total number of seeded cells by interpolating scaffold fluorescence readings within a standard curve [47].

2.8. Measurement of cell-mediated scaffold contraction

The diameter of each scaffold disk was measured at days 1, 4, 7, and 14 using standard drafting templates and normalized against scaffold diameter at time 0 to determine cell-mediated scaffold contraction [48].

2.9. Histology and immunohistochemistry

Scaffolds at days 7 and 14 of culture with TCs were fixed in 10% neutral buffered formalin for histological analysis. Two scaffolds per experimental group were embedded in paraffin and sequentially sliced (one through the longitudinal plane, one through the transverse plane per group) into 5 μm thick sections. Sections were stained with hematoxylin and eosin (H&E) to allow visualization of cells (purple) and scaffold struts (pink).

2.10. Quantitative assessment of scaffold strut and cell alignment

The scaffold pore alignment as well as alignment of TCs within scaffolds was quantitatively assessed using the OrientationJ plugin for Image J [49]. Scaffold strut alignment was measured from SEM images using the Distribution function within OrientationJ; 30x images taken in the longitudinal and transverse planes of bottom, middle, and top regions of the scaffold were analyzed for each freezing temperature (three scaffolds, nine total images for each plane). TC alignment within the scaffolds after 7 and 14 days in culture was measured from 10x images of H&E stained histology sections. The orientation angles of at least 450 TCs from nine distinct scaffold regions per scaffold variant were quantified for each sample using the Measure function. Strut and cell alignment is reported in terms of orientation angle (−90° – +90°) for specimens taken from the transverse and longitudinal planes (with 0° corresponding to the direction of hypothesized directional solidification in longitudinal sections).

2.11. Statistical analysis

One-way analysis of variance (ANOVA) was performed on pore size and shape, cell metabolic activity, cell number, and scaffold diameter data sets followed by Tukey-HSD post-hoc tests. Significance was set at $p < 0.05$. At least $n = 6$ scaffolds were analyzed at each time point for cell metabolic activity and scaffold diameter while $n = 6$ scaffolds were digested and assayed at each time point for cell number. Pore size and shape analysis was performed on transverse ($n = 3$) and longitudinal ($n = 3$) scaffold sections. Error is reported in figures as the standard error of the mean unless otherwise noted.

3. Results

3.1. Pore size and shape analysis

Directional solidification produced anisotropic CG scaffolds characterized by aligned pore tracks in the longitudinal plane comprised of aligned, ellipsoidal pores (Fig. 1(b–d)) regardless of freezing temperature. In contrast, pores in the transverse plane maintained a rounded morphology (Fig. 1(e–g)). Stereology analysis determined best-fit ellipses with an elongated AR in the longitudinal plane, but rounded AR in the transverse plane for each variant (Fig. 1(b–g), inset). Freezing temperature had a significant ($p < 0.0001$) effect on mean pore size and degree of anisotropy (Table 1). Due to the significant anisotropy, scaffold pore geometry is reported here as the mean pore size from the transverse (isotropic) plane and the pore aspect ratio (AR) in the transverse and longitudinal planes. Scaffolds fabricated at freezing temperatures of −10 °C, −40 °C, and −60 °C demonstrated statistically significant differences in pore sizes ($p < 0.001$): 243 ± 29, 152 ± 25, and 55 ± 18 μm. While mean pore size was consistent throughout the length of the 243 μm and 152 μm ($p > 0.05$) scaffolds, the bottom section of the 55 μm scaffold (closest to the freeze-dryer) showed a 35% reduction in pore size ($p < 0.05$) (Fig. 2(a)). All scaffolds had significantly ($p < 0.0001$) elongated pores in the longitudinal versus transverse planes (Table 1). Analysis of strut orientation showed struts preferentially aligned in the direction of the heat transfer gradient during solidification (longitudinal plane, 0°) with a lack preferential strut alignment in the transverse plane (Fig. 2(b)), confirming presence of aligned contact guidance cues. The isotropic scaffold control had an isotropic structure (AR: 1.05 ± 0.03) with a mean pore size (combined transverse and longitudinal planes) of 87 ± 10 μm [42].

3.2. Scaffold contraction in isotropic versus anisotropic CG scaffolds

The CG scaffold variants showed significant contraction over the 14 day culture period (Fig. 3). At 1 day all groups maintained a normalized diameter greater than 0.95 with no significant difference between variants ($p = 0.06$). However for all subsequent time points

the isotropic control scaffold showed significantly greater contraction than all anisotropic variants (day 4: $p < 0.05$; days 7, 14: $p < 0.01$). By day 14, the anisotropic scaffold with the largest pores (243 μm) showed significantly reduced contraction compared to the other anisotropic scaffolds as well as the isotropic control ($p = 0.01$).

3.3. Tendon cell attachment and proliferation

DNA quantification showed that there was significant TC proliferation within the scaffolds (Fig. 4(a)). At day 1 between 40 and 55% of the originally seeded TCs remained attached to the scaffold network, consistent with previous results [25]. Subsequently, all scaffolds supported significant TC proliferation; for each remaining time point the aligned scaffolds contained significantly greater numbers of TCs than the isotropic control ($p < 0.05$) with no significant difference in TC number observed between aligned groups at any time point.

3.4. Tendon cell metabolic activity

For all time points the aligned scaffold variants all supported significantly higher TC metabolic activity compared to the isotropic control (day 1: $p < 0.0001$; days 4, 7: $p < 0.001$; day 14: $p < 0.01$) (Fig. 4(b)). Starting at day 4 and continuing through the rest of the experiment, a pore size dependent effect was observed on TC metabolic activity within the anisotropic scaffolds, with the largest scaffold (pore size: 243 μm) showing the highest metabolic activity (day 4: $p < 0.0001$; day 7: $p < 0.01$; day 14: $p < 0.001$). At day 7, a direct correlation between anisotropic pore size and TC metabolic activity was observed (minimum $p < 0.02$ for all groups).

3.5. Tendon cell distribution within the scaffold

Histology specimens taken from transverse sections through the scaffolds at day 14 showed that while there was no significant difference in total number of TCs in the three anisotropic CG scaffolds (Fig. 4(a)), there was a marked difference in TC penetration into the scaffold network that was dependent on scaffold pore size. While TCs in the scaffold with the smallest pore size (55 μm) were observed to be aggregated at the edge of the scaffold with little to no penetration into the scaffold network (Fig. 4(c)), TCs were more evenly distributed throughout the scaffolds with larger pore size scaffolds (152, 243 μm, Fig. 4(d–e)).

3.6. Tendon cell alignment within anisotropic and isotropic CG scaffolds

H&E stained histology specimens taken from the longitudinal and transverse planes of each scaffold were analyzed to determine the relationship between scaffold microstructural cues and TC alignment. Frequency plots of TC orientation angle (−90° - +90°) for a minimum of 450 TCs in the transverse and longitudinal planes of each variant was generated with consistent results seen at days 7 and 14. In the transverse plane where both the anisotropic scaffolds and isotropic controls display rounded pores, TCs orientation angle was uniformly distributed (Fig. 5(a,c)). In the longitudinal plane of the isotropic control TCs again showed a uniform distribution of orientation angles. However, at both days 7 and 14 a strong correlation was observed between TC orientation angleand scaffold anisotropy in all anisotropic scaffold variants (Fig. 5(b,d)). Within anisotropic scaffolds, TCs were significantly ($p < 0.02$) more likely to be oriented in the direction of scaffold pore alignment and directional solidification (between −10° and +10°) and less likely to be oriented in the orthogonal direction (between ±80° and ±90°) than the isotropic control.

3.7. Tendon cell chemotaxis in response to PDGF-BB and IGF-1 supplementation

TC chemotaxis into the large pore (243 μm) anisotropic CG scaffold in response to PDGF-BB (10, 50, or 100 ng/mL) and IGF-1 (50, 100, or 500 ng/mL) was assessed using a

modified Transwell assay (Fig. 6(a)). All three IGF-1 doses led to significantly higher numbers of recruited TCs within the scaffold after 24 h compared to the control ($p < 0.05$) with no statistical differences between doses. IGF-1 concentrations of 50 and 100 ng/mL also led to a significant increase in TC metabolic activity versus the non-supplemented controls ($p < 0.05$); the 500 ng/mL IGF-1 group also showed increased TC metabolic activity compared to control, but the difference was not quite significant ($p = 0.07$) (Fig. 6(c)). The number of recruited TCs showed a dose-dependent response to PDGF-BB supplementation, with 100 ng/mL supplementation recruiting a significantly greater number of TCs compared to the non-supplemented control and the lower PDGF-BB concentrations ($p < 0.05$) (Fig. 6(b)). All three PDGF-BB groups showed significantly increased TC metabolic activity compared to the non-supplemented control ($p < 0.05$) as well as a significant dose-dependence ($p < 0.05$ for all groups) (Fig. 6(c)). The presence (chemokinesis condition) or absence (chemotaxis condition) of growth factor in the top compartment of the Transwell membrane did not have a significant effect on the number of TCs recruited into the scaffold at 24 h (PDGF-BB 50 ng/mL; $p = 0.93$; data not shown).

3.8. Tendon cell viability and metabolic activity with PDGF-BB and IGF-1 supplementation

The presence of PDGF-BB or IGF-1 (100 ng/mL dose for either, chosen as a result of Transwell assay results) had a significant effect on TC proliferation and metabolic activity out to 7 days in the anisotropic CG scaffolds. PDGF-BB supplemented scaffolds showed a significant ($p < 0.05$) increase in TC number at each time point compared to non-supplemented controls for all scaffolds except for the 243 μm scaffolds at day 1 and the 55 μm scaffolds at day 7 which had non-significant increases (Fig. 7(a)). At all time points the 152 μm scaffold with PDGF-BB supplementation had significantly higher TC number that the other pore sizes ($p < 0.05$). For all scaffolds and time points, PDGF-BB supplementation significantly ($p < 0.05$) increased TC metabolic activity compared to non-supplemented controls (Fig. 7(b)). Further, TC metabolic activity in response to PDGF-BB supplementation was significantly ($p < 0.05$) increased in the medium (152 μm) and large (243 μm) pore scaffolds compared to the 55 μm scaffolds at the longer culture periods (Fig. 7(b)). For the most part, IGF-1 supplemented scaffolds showed increased TC numbers and metabolic activity compared to non-supplemented controls, particularly at the early time points (day 1, 4) (Fig. 8(a)); there were no significant differences in TC number between the IGF-1 experimental groups at day 7 ($p = 0.49$). While IGF-1 supplemented scaffolds also displayed significantly ($p < 0.05$) higher TC metabolic activity compared to the non-supplemented control for each scaffold and at all three time points, TC metabolic activity decreased over time even with supplementation and the relative increase at each time point was considerably smaller than that seen with PDGF-BB supplementation (Fig. 8(b)).

4. Discussion

This paper describes integration of 3D contact guidance cues with PDGF-BB and IGF-1 supplementation within an anisotropic CG scaffold for tendon tissue engineering. We have developed a directional heat transfer approach to fabricate a homologous series of highly porous CG scaffolds with longitudinally aligned microstructure mimicking elements of the native tendon physiology. The homologous series was comprised of scaffolds with a constant relative density ($\rho^*/\rho_s = 0.006$) but with pores relatively small (55 μm), medium (152 μm), and large (243 μm) in size compared to native equine tendon fibroblasts, with documented elongated lengths greater than 100–125 μm [27]. In addition to showing a significant influence of aligned pore microstructure on TC penetration into the scaffold as well as subsequent alignment, proliferation, and metabolic activity, we also showed that PDGF-BB and IGF-1 supplementation has beneficial effects on TC recruitment and resultant bioactivity.

We hypothesized that directional solidification would create CG scaffolds with highly aligned, anisotropic microstructures. We created a unique multi-part mold comprised of a PTFE body and thin (1/16″) copper bottom (Fig. 1(a)) where the significant thermal conductivity mismatch between phases (k_{Cu}/k_{PTFE} ~ 1600) would induce unidirectional heat transfer during solidification. Previous work has used controlled solidification to produce CG scaffolds with axially-oriented pore tracks for peripheral nerve applications; however these materials were fabricated from a single phase tubular mold by controlling the rate of submersion into a chilled refrigerant bath, a process that created aligned pore tracks of non-elongated pores less than 30 μm in size [50], limiting their applicability for orthopedic tissue regeneration. Here we rapidly froze the CG suspension by placing the thermally mismatched mold directly onto a pre-cooled freeze-dryer shelf. Based on previous results indicating that lower freezing temperatures induce decreased pore size [25,41,51], we chose freezing temperatures of −10, −40, and −60 °C to create pore morphologies with features (pores) relatively small, medium, and large compared to individual equine tendon fibroblasts. The resultant scaffolds (6 mm dia., 15 mm length) displayed significant pore alignment and anisotropy. SEM images (Fig. 1(b–d)) as well as best-fit ellipses of the mean pore (Fig. 1(b–d, inset)) as determined via stereology showed that regardless of solidification temperature, in the longitudinal plane pores were aligned and elongated in the direction of heat transfer. Additionally, qualitative SEM (Fig. 1(e–g)) and quantitative stereology (Fig. 1(e–g, inset)) analyses in the transverse plane indicated pores were round and isotropic. Consistent with previous work, we demonstrated that freezing temperature had a significant effect on mean pore size with warmer freezing temperatures leading to larger pores (Table 1). Pore size and shape was found shown to be uniform throughout the depth (15 mm) of the cylindrical scaffolds with the exception of the 55 μm variant, which showed a reduced pore size only in the region of the scaffold closest to the copper plate (the initial region of the suspension to solidify). Additionally, while the pore aspect ratio was found to be rounded in the transverse plane for all variants, in the longitudinal plane the pore aspect ratio was significantly elongated (Table 1) in the direction of heat transfer throughout the scaffold depth. However, the degree of pore elongation was reduced in the 55 μm pore size scaffold relative to the 152 μm and 243 μm in the region closest to the copper plate. It is likely that the reduced size and aspect ratio in the bottom region of the 55 μm scaffolds (fabricated at 60 −C) was due to increased resistance to mass transfer as a result ° of the CG suspension viscosity increasing at its glass transition temperature (−42 °C) [51], something not observed at the warmer freezing temperatures above the glass transition.

A histogram depicting strut alignment within the transverse and longitudinal planes of the anisotropic scaffold variants (Fig. 2(b)) showed significant strut alignment due to directional solidification in the longitudinal plane (0° corresponding the direction of heat transfer), but not in the transverse plane. We then determined whether scaffold contact guidance cues translated to TCs seeded within the network. After both 1 and 2 weeks in culture, no preferential alignment was observed for TCs seeded in the isotropic control in either the transverse or longitudinal planes (Fig. 5). However, significant TC alignment in the direction of the structural contact guidance cues was observed in the longitudinal plane of the anisotropic scaffolds relative to the isotropic control (Fig. 5(b,d)) and to TCs in the transverse plane of the same isotropic scaffolds (Fig. 5(a,c)). Further, the number of TCs oriented in the direction orthogonal to contact guidance cues (±90°) in the longitudinal plane of the anisotropic scaffolds was reduced compared to even the isotropic control, which demonstrated an even distribution of cell orientation angles (Fig. 5(b,d)). Taken together, these results indicate that directional solidification enables fabrication of highly aligned, 3D scaffold microstructures that present significant contact guidance cues to cells within their network. There does not appear to be any trend relating cell alignment to pore size, though pore size was a significant regulator of TC proliferation and metabolic activity. Although the influence of material microstructural features on cell alignment in 2D systems has been

previously shown [26,27], this is the first report quantifying induced cell alignment within three-dimensional anisotropic CG scaffolds.

Cellular solids tools provide a framework to consider the microenvironment surrounding TCs in the CG scaffolds used in this study [4,5,24,25,44,52]. All scaffolds (isotropic, anisotropic) were fabricated with a constant relative density (0.006) but distinct pore sizes (*d*). We considered four distinct effects of scaffold microstructure using cellular solids tools. *Scaffold permeability* dictates diffusive transport of cytokines, nutrients, and waste throughout the scaffold, making it a critical factor to optimize [53,54]; CG scaffold permeability has been previously shown to increase proportionally with scaffold d^2 [24]. *Scaffold specific surface area* (*SA/V*), the total scaffold surface area divided by its volume, dictates the amount of surface available for cells to attach; *SA/V* has been shown to be inversely proportional to scaffold *d* and an integral factor affecting cell attachment [25,52]. While the scaffolds display an open-cell structure, *steric hindrance* becomes a factor with decreasing pore size. Finally, we have previously shown that while overall scaffold modulus is proportional to relative density not pore size, the *flexural rigidity* (resistance to bending) of individual struts within the scaffold network increases proportional with d^2 [4]. Our results here can be considered as a function of these four competing factors. Pore size must be optimized so that there is ample surface area for cells to adhere and proliferate while not sterically hindering their recruitment into the scaffold and while maintaining adequate permeability; pore AR further influences the relative distribution of solid content, hence scaffold modulus in the directions of the major and minor axes of the elongated pores [23]. Cell-mediated contraction can significantly alter scaffold microstructure; TCs are highly contractile and have been previously shown to significantly contract CG scaffolds [55]. Despite a high degree of crosslinking, all scaffolds were significantly contracted in the transverse plane during 14 day culture (Fig. 3). However, anisotropic scaffolds of all pore sizes contracted to a significantly lesser extent compared to the isotropic control, likely due to both the differential distribution of CG content (hence modulus) in the transverse plane of isotropic versus anisotropic scaffolds as well as the increased alignment of TCs within the anisotropic scaffolds in the longitudinal direction (Fig. 5). As would be predicted by cellular solids analysis, the degree of TC-induced contraction was pore size dependent with the large pore (243 μm) anisotropic scaffold composed of longer, thicker struts with the largest strut flexural rigidity being most resistant to radial contraction at 14 days.

The degree of TC proliferation, metabolic activity, and penetration into the scaffold can also be considered in the light of competing design criteria. Despite the fact that the majority of TCs are terminally differentiated fibroblasts, CG scaffolds display excellent bioactivity with TC number after 14 days reaching approximately twice the number of seeded cells. Though not significant, the number of TCs on the aligned scaffolds at day 1 correlated directly with *SA/V* (Fig. 4(a)), suggesting that scaffold microstructure directly affects initial TC attachment via ligand availability. While no correlation was observed at later time points between TC number and anisotropic scaffold pore size, histological analysis at day 14 (Fig. 4(c–e)) indicated that while in the smallest pore size (55 μm) TCs remained aggregated at the scaffold edge, TCs were more evenly distributed through the strut network in the larger pore size (152, 243 μm) scaffolds. Further, a significant influence of anisotropic scaffold pore size was seen on TC metabolic activity where the 243 μm scaffold consistently showed higher metabolic activity (Fig. 4(b)). The alamarBlue assay is a measure of mitochondrial metabolic activity and an indicator of overall cell health. Despite no differences in TC number between anisotropic groups at each time point, the decrease in metabolic activity with decreasing pore size is likely due to decreased scaffold permeability, a factor aggravated by increased scaffold contraction with decreasing pore size. These results suggest that pore size mediated *SA/V*, steric hindrance, and permeability affect TC recruitment into the scaffold as well as subsequent proliferation and metabolic activity.

After it was demonstrated that aligned CG scaffolds could support long-term TC viability, we investigated the potential of growth factor supplementation to increase cell recruitment into what were originally acellular materials. It was hypothesized that PDGF-BB and IGF-1, both known chemoattractants of mesenchymal cells [33–35], would aid TC recruitment. Using the large pore size (243 μm) scaffold, we used a modified Transwell membrane assay to determine PDGF-BB and IGF-1 concentrations that induced TC recruitment. The Transwell experiments initially compared TC chemotaxis (growth factor present in bottom compartment only) versus TC chemokinesis (growth factor present in equal concentrations in both the top and bottom compartments), and showed no significant differences in migrated TC number or resultant metabolic activity at 24 h for both PDGF-BB and IGF-1. A mathematical model for PDGF gradient sensing by fibroblasts developed by Haugh *et al.* offers a possible explanation. The authors found that sharp gradients do not necessarily improve migration; the simple presence of a therapeutic dose of PDGF may be sufficient to encourage migration [56,57]. We also found that PDGF-BB elicited a significant increase in migrated TC number over a non-supplemented control, but only for the 100 ng/mL dose, while IGF-1 significantly increased migrated TC number for all tested doses (Fig. 6(b)). PDGF-BB further elicited dose-dependent increases in TC metabolic activity, where the high PDGF-BB dose group showed metabolic activity levels nearly three times the amount of the control. IGF-1 showed significant increases in metabolic activity for the two lower doses, but no dose-dependence (Fig. 6(c)).

After identifying therapeutic dosages for PDGF-BB and IGF-1 (100 ng/mL), we determined their effect on TC recruitment, proliferation and metabolic activity over a 7 day culture assay. PDGF-BB elicited significant increases in TC number at each time point (Fig. 7(a)) except for the 243 μm group at day 1 and the 55 μm group at day 7. Additionally, the 152 μm group had significantly higher TC number than the other aligned variants at all time points, suggesting a tradeoff between scaffold *SA/V* and permeability. Significant increases in TC number were observed for all IGF-1 supplemented groups compared to non-supplemented controls at days 1 and 4 (except for the 243 μm group at day 1) (Fig. 8(a)). Both PDGF-BB and IGF-1 supplemented scaffolds showed dramatically higher TC metabolic activity compared to the non-supplemented controls at all time points (over ten-fold at days 4 and 7 for PDGF-BB; Figs 7(b), 8(b)). PDGF-BB supplementation showed the greatest increase on TC metabolic activity in the largest pore scaffolds (152, 243 μm), suggesting that while TC number was increased in the medium pore scaffold, cells in the largest pore scaffold showed higher per capita metabolic activity. IGF-1 supplementation induced a lesser response that PDGF-BB, thought the smallest pore size scaffold displayed a significantly lower TC metabolic activity at all three time points. These results again suggest the tradeoff between scaffold *SA/V* and permeability on the number and metabolic health of TCs within the scaffold network.

While this work presents the effects of soluble factors on TC behavior, it is well understood that many biomolecules are natively ECM-immobilized [28]. Further, bolus delivery of biomolecules is not practical or efficient for *in vivo* translation [7]. Our lab has recently developed a direct photolithographic method to pattern covalently-immobilized biomolecules within CG scaffolds [42]; ongoing work is applying this strategy to pattern and immobilize growth factors to the anisotropic scaffolds developed here. We also recognize the necessity to improve scaffold mechanical properties to resist TC contraction and endure *in vivo* mechanical loading. We are currently studying CG scaffold with higher relative densities, hence significantly higher elastic moduli, as well as integrating CG membranes to the scaffold to create core-shell composites mimicking mechanically efficient structures in nature to improve construct tensile strength.

5. Conclusions

We introduce here highly porous CG scaffolds with longitudinally aligned, elongated pore microstructures mimicking tendon and other anisotropic tissues over a wide range of pore sizes. This work establishes aligned CG scaffolds coupled with PDGF-BB and IGF-1 as a promising biomaterial system for tendon regenerative medicine applications. Analysis of TC viability in these scaffolds indicates that anisotropic variants can support increased cell number, alignment, and metabolic activity compared to isotropic scaffolds. Additionally, while scaffolds with smaller pore sizes can initially support attachment of greater TC numbers due to increased *SA/V*, scaffolds with larger pores support greater TC proliferation and metabolic activity due to higher permeability. Larger pores also reduce TC aggregation on the edges of, and enhance penetration into, the scaffolds, suggesting an aligned CG scaffold with larger pores (≥150 μm) may be preferred for tendon tissue engineering. We have also shown that the growth factors PDGF-BB and IGF-1 can increase TC migratory capacity as well as recruitment into and metabolic activity within anisotropic CG scaffolds. In particular, PDGF-BB supplementation was found to be a promising target to increase overall CG scaffold bioactivity for tendon tissue engineering applications. Future work will explore additional soluble factors and exploit surface immobilization techniques to identify combinations of contact guidance cues and biomolecule supplementation that improve TC gene expression and matrix biosynthesis. The materials developed here are also likely to be useful as 3D templates for a range of anisotropic tissues, including ligament and cardiac tissue.

Acknowledgments

The authors would like to acknowledge Dr. Allison Stewart and Dr. Matthew Stewart (Veterinary Sciences, UIUC) for providing equine tendon cells, Karen Doty (Veterinary Sciences, UIUC) for sectioning of GMA embedded samples, Donna Epps for sectioning and staining of paraffin embedded samples, and Dr. Charles Schroeder (ChBE, UIUC) for the use of his fluorescence spectrophotometer. We are grateful for the funding for this study provided by the Chemistry–Biology Interface Training Program NIH NIGMS T32GM070421 (SRC), the Chemical and Biomolecular Engineering Dept. (BAH), and the Institute for Genomic Biology (BAH) at the University of Illinois at Urbana-Champaign. This research was carried out in part in the Frederick Seitz Materials Research Laboratory Central Facilities, University of Illinois, which are partially supported by the U.S. Department of Energy under grants DE-FG02-07ER46453 and DE-FG02-07ER46471.

References

[1]. Yannas IV, Lee E, Orgill DP, Skrabut EM, Murphy GF. Synthesis and characterization of a model extracellular matrix that induces partial regeneration of adult mammalian skin. Proc Natl Acad Sci U S A. 1989; 86:933–7. [PubMed: 2915988]

[2]. Harley BA, Spilker MH, Wu JW, Asano K, Hsu HP, Spector M, et al. Optimal degradation rate for collagen chambers used for regeneration of peripheral nerves over long gaps. Cells Tissues Organs. 2004; 176:153–65. [PubMed: 14745243]

[3]. Yannas, IV. Tissue and organ regeneration in adults. Springer; New York: 2001.

[4]. Harley BA, Kim HD, Zaman MH, Yannas IV, Lauffenburger DA, Gibson LJ. Microarchitecture of three-dimensional scaffolds influences cell migration behavior via junction interactions. Biophys J. 2008; 95:4013–24. [PubMed: 18621811]

[5]. Harley BA, Freyman TM, Wong MQ, Gibson LJ. A new technique for calculating individual dermal fibroblast contractile forces generated within collagen-GAG scaffolds. Biophys J. 2007; 93:2911–22. [PubMed: 17586570]

[6]. Harley BAC, Gibson LJ. In vivo and in vitro applications of collagen-GAG scaffolds. Chem Eng J. 2008; 137:102–21.

[7]. Harley BA, Lynn AK, Wissner-Gross Z, Bonfield W, Yannas IV, Gibson LJ. Design of a multiphase osteochondral scaffold III: fabrication of layered scaffolds with continuous interfaces. J Biomed Mater Res A. 2010; 92:1078–93. [PubMed: 19301263]

[8]. Harley BA, Lynn AK, Wissner-Gross Z, Bonfield W, Yannas IV, Gibson LJ. Design of a multiphase osteochondral scaffold. II. Fabrication of a mineralized collagen-glycosaminoglycan scaffold. J Biomed Mater Res A. 2010; 92:1066–77. [PubMed: 19301274]

[9]. James R, Kesturu G, Balian G, Chhabra AB. Tendon: Biology, biomechanics, repair, growth factors, and evolving treatment options. J Hand Surg Am. 2008; 33A:102–12. [PubMed: 18261674]

[10]. Liu Y, Ramanath HS, Wang DA. Tendon tissue engineering using scaffold enhancing strategies. Trends Biotechnol. 2008; 26:201–9. [PubMed: 18295915]

[11]. Butler DL, Juncosa-Melvin N, Boivin GP, Galloway MT, Shearn JT, Gooch C, et al. Functional tissue engineering for tendon repair: a multidisciplinary strategy using mesenchymal stem cells, bioscaffolds, and mechanical stimulation. J Orthop Res. 2008; 26:1–9. [PubMed: 17676628]

[12]. Xu Y, Murrell GA. The basic science of tendinopathy. Clin Orthop Relat Res. 2008; 466:1528–38. [PubMed: 18478310]

[13]. Soo C, Beanes SR, Hu FY, Zhang XL, Dang C, Chang G, et al. Ontogenetic transition in fetal wound transforming growth factor-beta regulation correlates with collagen organization. Am J Pathol. 2003; 163:2459–76. [PubMed: 14633618]

[14]. Cole DW, Ginn TA, Chen GJ, Smith BP, Curl WW, Martin DF, et al. Cost comparison of anterior cruciate ligament reconstruction: autograft versus allograft. Arthroscopy. 2005; 21:786–90. [PubMed: 16012490]

[15]. Harley BAC, Gibson LJ. In vivo and in vitro applications of collagen-GAG scaffolds. Chem Eng J. 2008; 137:102–21.

[16]. Li X, Xie J, Lipner J, Yuan X, Thomopoulos S, Xia Y. Nanofiber scaffolds with gradations in mineral content for mimicking the tendon-to-bone insertion site. Nano Lett. 2009; 9:2763–8. [PubMed: 19537737]

[17]. Moffat KL, Kwei AS, Spalazzi JP, Doty SB, Levine WN, Lu HH. Novel nanofiber-based scaffold for rotator cuff repair and Augmentation. Tissue Eng Part A. 2009; 15:115–26. [PubMed: 18788982]

[18]. Lu HH, Cooper JA Jr, Manuel S, Freeman JW, Attawia MA, Ko FK, et al. Anterior cruciate ligament regeneration using braided biodegradable scaffolds: in vitro optimization studies. Biomaterials. 2005; 26:4805–16. [PubMed: 15763260]

[19]. Kim YT, Haftel VK, Kumar S, Bellamkonda RV. The role of aligned polymer fiber-based constructs in the bridging of long peripheral nerve gaps. Biomaterials. 2008; 29:3117–27. [PubMed: 18448163]

[20]. Engelmayr GC Jr, Cheng M, Bettinger CJ, Borenstein JT, Langer R, Freed LE. Accordion-like honeycombs for tissue engineering of cardiac anisotropy. Nat Mater. 2008; 7:1003–10. [PubMed: 18978786]

[21]. Xie J, Li X, Lipner J, Manning CN, Schwartz AG, Thomopoulos S, et al. Aligned-to-random" nanofiber scaffolds for mimicking the structure of the tendon-to-bone insertion site. Nanoscale. 2010; 2:923–6. [PubMed: 20648290]

[22]. Yin Z, Chen X, Chen JL, Shen WL, Hieu Nguyen TM, Gao L, et al. The regulation of tendon stem cell differentiation by the alignment of nanofibers. Biomaterials. 2010; 31:2163–75. [PubMed: 19995669]

[23]. Gibson, LJ.; Ashby, MF. Cellular solids: structure and properties. 2nd ed. Cambridge University Press; Cambridge, U.K: 1997.

[24]. O'Brien FJ, Harley BA, Waller MA, Yannas IV, Gibson LJ, Prendergast PJ. The effect of pore size on permeability and cell attachment in collagen scaffolds for tissue engineering. Technol Health Care. 2007; 15:3–17. [PubMed: 17264409]

[25]. O'Brien FJ, Harley BA, Yannas IV, Gibson LJ. The effect of pore size on cell adhesion in collagen-GAG scaffolds. Biomaterials. 2005; 26:433–41. [PubMed: 15275817]

[26]. Zhu J, Li J, Wang B, Zhang WJ, Zhou G, Cao Y, et al. The regulation of phenotype of cultured tenocytes by microgrooved surface structure. Biomaterials. 2010; 31:6952–8. [PubMed: 20638974]

[27]. Kapoor A, Caporali EH, Kenis PJ, Stewart MC. Microtopographically patterned surfaces promote the alignment of tenocytes and extracellular collagen. Acta Biomater. 2010; 6:2580–9. [PubMed: 20045087]

[28]. Molloy T, Wang Y, Murrell G. The roles of growth factors in tendon and ligament healing. Sports Med. 2003; 33:381–94. [PubMed: 12696985]

[29]. Thomopoulos S, Harwood FL, Silva MJ, Amiel D, Gelberman RH. Effect of several growth factors on canine flexor tendon fibroblast proliferation and collagen synthesis in vitro. J Hand Surg Am. 2005; 30A:441–7. [PubMed: 15925149]

[30]. Costa MA, Wu C, Pham BV, Chong AKS, Pham HM, Chang J. Tissue engineering of flexor tendons: optimization of tenocyte proliferation using growth factor supplementation. Tissue Eng. 2006; 12:1937–43. [PubMed: 16889523]

[31]. Yoshikawa Y, Abrahamsson SO. Dose-related cellular effects of platelet-derived growth factor-BB differ in various types of rabbit tendons in vitro. Acta Orthop Scand. 2001; 72:287–92. [PubMed: 11480607]

[32]. Abrahamsson SO, Lundborg G, Lohmander LS. Recombinant human insulin-like growth factor-I stimulates in vitro matrix synthesis and cell proliferation in rabbit flexor tendon. J Orthop Res. 1991; 9:495–502. [PubMed: 2045976]

[33]. Li Y, Yu X, Lin S, Li X, Zhang S, Song YH. Insulin-like growth factor 1 enhances the migratory capacity of mesenchymal stem cells. Biochem Biophys Res Commun. 2007; 356:780–4. [PubMed: 17382293]

[34]. Ponte AL, Marais E, Gallay N, Langonne A, Delorme B, Herault O, et al. The in vitro migration capacity of human bone marrow mesenchymal stem cells: comparison of chemokine and growth factor chemotactic activities. Stem Cells. 2007; 25:1737–45. [PubMed: 17395768]

[35]. Ozaki Y, Nishimura M, Sekiya K, Suehiro F, Kanawa M, Nikawa H, et al. Comprehensive analysis of chemotactic factors for bone marrow mesenchymal stem cells. Stem Cells Dev. 2007; 16:119–29. [PubMed: 17348810]

[36]. Dines JS, Grande DA, Dines DM. Tissue engineering and rotator cuff tendon healing. J Shoulder Elbow Surg. 2007; 16:S204–7. [PubMed: 17524676]

[37]. Steinert AF, Palmer GD, Capito R, Hofstaetter JG, Pilapil C, Ghivizzani SC, et al. Genetically enhanced engineering of meniscus tissue using ex vivo delivery of transforming growth factor-beta 1 complementary deoxyribonucleic acid. Tissue Eng. 2007; 13:2227–37. [PubMed: 17561802]

[38]. Capito RM, Spector M. Collagen scaffolds for nonviral IGF-1 gene delivery in articular cartilage tissue engineering. Gene Ther. 2007; 14:721–32. [PubMed: 17315042]

[39]. Madaghiele M, Sannino A, Yannas IV, Spector M. Collagen-based matrices with axially oriented pores. J Biomed Mater Res A. 2008; 85A:757–67. [PubMed: 17896767]

[40]. Harley BA, Hastings AZ, Yannas IV, Sannino A. Fabricating tubular scaffolds with a radial pore size gradient by a spinning technique. Biomaterials. 2006; 27:866–74. [PubMed: 16118016]

[41]. O'Brien FJ, Harley BA, Yannas IV, Gibson L. Influence of freezing rate on pore structure in freeze-dried collagen-GAG scaffolds. Biomaterials. 2004; 25:1077–86. [PubMed: 14615173]

[42]. Martin TA, Caliari SR, Williford PD, Harley BA, Bailey RC. The generation of biomolecular patterns in highly porous collagen-GAG scaffolds using direct photolithography. Biomaterials. 2011; 32:3949–57. [PubMed: 21397322]

[43]. Olde Damink LH, Dijkstra PJ, van Luyn MJ, van Wachem PB, Nieuwenhuis P, Feijen J. Cross-linking of dermal sheep collagen using a water-soluble carbodiimide. Biomaterials. 1996; 17:765–73. [PubMed: 8730960]

[44]. Harley BA, Leung JH, Silva EC, Gibson LJ. Mechanical characterization of collagen-glycosaminoglycan scaffolds. Acta Biomater. 2007; 3:463–74. [PubMed: 17349829]

[45]. Freyman TM, Yannas IV, Gibson LJ. Cellular materials as porous scaffolds for tissue engineering. Prog Mater Sci. 2001; 46:273–82.

[46]. Kim YJ, Sah RL, Doong JY, Grodzinsky AJ. Fluorometric assay of DNA in cartilage explants using Hoechst 33258. Anal Biochem. 1988; 174:168–76. [PubMed: 2464289]

[47]. Tierney CM, Jaasma MJ, O'Brien FJ. Osteoblast activity on collagen-GAG scaffolds is affected by collagen and GAG concentrations. J Biomed Mater Res A. 2009; 91:92–101. [PubMed: 18767061]

[48]. Spilker MH, Asano K, Yannas IV, Spector M. Contraction of collagen-glycosaminoglycan matrices by peripheral nerve cells in vitro. Biomaterials. 2001; 22:1085–93. [PubMed: 11352089]

[49]. Fonck E, Feigl GG, Fasel J, Sage D, Unser M, Rufenacht DA, et al. Effect of aging on elastin functionality in human cerebral arteries. Stroke. 2009; 40:2552–6. [PubMed: 19478233]

[50]. Loree, HM.; Yannas, IV.; Mikic, B.; Chang, AS.; Perutz, SM.; Norregaard, TV., et al. A freeze-drying process for fabrication of polymeric bridges for peripheral nerve regeneration. Proc 15th Ann Northeast Bioeng Conf; 1989. p. 53-4.

[51]. Haugh MG, Murphy CM, O'Brien FJ. Novel freeze-drying methods to produce a range of collagen-glycosaminoglycan scaffolds with tailored mean pore sizes. Tissue Eng Part C Methods. 2010; 16:887–94. [PubMed: 19903089]

[52]. Murphy CM, Haugh MG, O'Brien FJ. The effect of mean pore size on cell attachment, proliferation and migration in collagen-glycosaminoglycan scaffolds for bone tissue engineering. Biomaterials. 2010; 31:461–6. [PubMed: 19819008]

[53]. Prendergast PJ, Huiskes R, Soballe K. ESB Research Award 1996. Biophysical stimuli on cells during tissue differentiation at implant interfaces. J Biomech. 1997; 30:539–48. [PubMed: 9165386]

[54]. Agrawal CM, McKinney JS, Lanctot D, Athanasiou KA. Effects of fluid flow on the in vitro degradation kinetics of biodegradable scaffolds for tissue engineering. Biomaterials. 2000; 21:2443–52. [PubMed: 11055292]

[55]. Torres DS, Freyman TM, Yannas IV, Spector M. Tendon cell contraction ofcollagen-GAG matrices in vitro: effect of cross-linking. Biomaterials. 2000; 21:1607–19. [PubMed: 10885733]

[56]. Schneider IC, Haugh JM. Mechanisms of gradient sensing and chemotaxis: conserved pathways, diverse regulation. Cell Cycle. 2006; 5:1130–4. [PubMed: 16760661]

[57]. Haugh JM. Deterministic model of dermal wound invasion incorporating receptor-mediated signal transduction and spatial gradient sensing. Biophys J. 2006; 90:2297–308. [PubMed: 16415056]

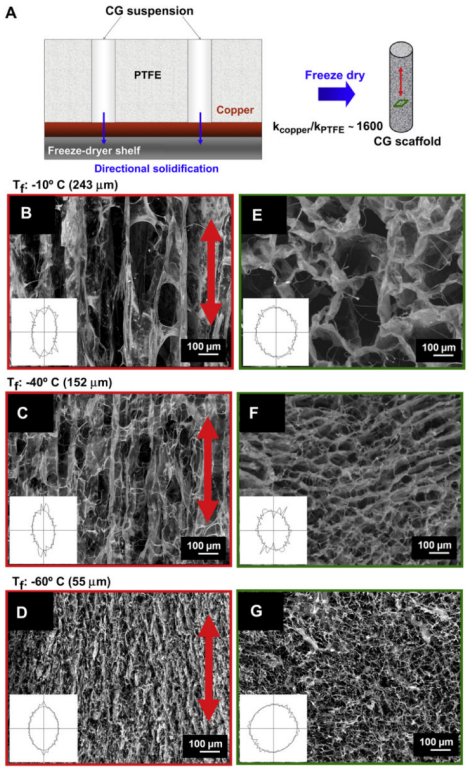

Fig. 1.

Directional solidification approach to fabricate aligned CG scaffolds. A) A two component mold with a significant mismatch in thermal conductivity is used to promote unidirectional heat transfer. B–D) SEM image of scaffold microstructure in the longitudinal plane for scaffolds fabricated at freezing temperature (Tf) of B) −10 °C, C) −40 °C and D) −60 °C showing a longitudinally aligned scaffold comprised of ellipsoidal pores. Red arrow: direction of heat transferE–G) SEM image of scaffold microstructure in the transverse plane for same scaffolds fabricated at E) −10 °C, F) −40 °C, and G) −60 °C. Inset: stereology determined best-fit ellipse representation of mean pore shape. (For interpretation of the references to colour in this figure legend, the reader is referred to the web version of this article.)

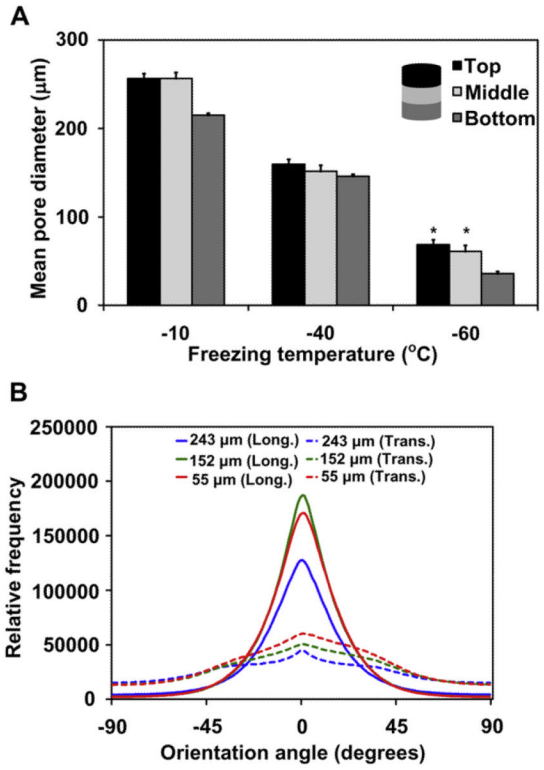

Fig. 2.

Distribution of pore size and strut orientation within the aligned scaffold variants. A) Transverse pore sizes for scaffolds fabricated at −10 °C, −40 °C, and −60 °C as determined from the bottom, middle, and top 5 mm sections of the overall 15 mm scaffold ($n = 3$). (*) significance ($p < 0.05$) compared to bottom region. B) Histogram of scaffold strut orientation angles within the transverse (dotted line) and longitudinal (solid line) planes of the aligned scaffold variants.

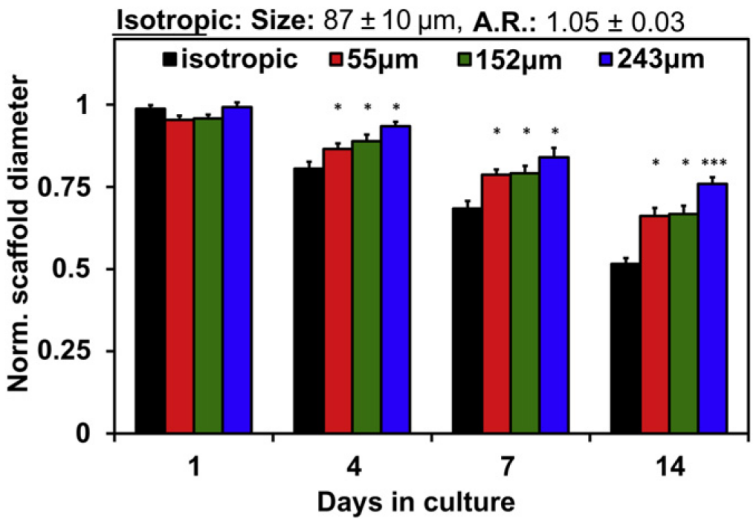

Fig. 3.

TC-mediated scaffold contraction. Scaffold diameter (normalized by initial diameter) at 1, 4, 7, and 14 days for the aligned (55 μm, 152 μm, 243 μm) scaffold variants compared to an isotropic CG scaffold (pore size: 87 μm, A.R: 1.05). (*) significance ($p < 0.05$) compared to isotropic group, (***) significance ($p < 0.05$) compared to all other groups at given time point. Data expressed as mean ± SEM, $n = 6$.

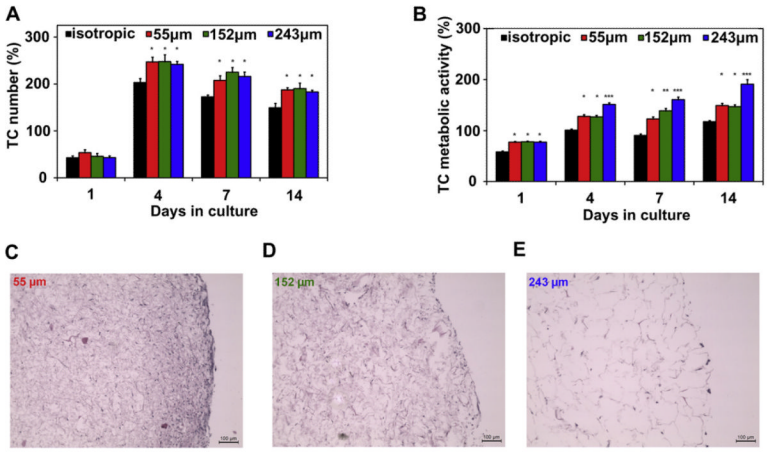

Fig. 4.

TC proliferation and metabolic activity without growth factor supplementation. A) TC number and B) TC metabolic activity at 1, 4, 7, and 14 days in isotropic and aligned (55 μm, 152 μm, 243 μm) scaffold variants. C–E) H&E stained cross-sections after 14 day culture demonstrate decreasing cell aggregation at scaffold edges with increasing pore size: C) 55 μm D) 152 μm E) 243 μm (*) significance ($p < 0.05$) compared to isotropic group, (**) significance ($p < 0.05$) compared to 55 μm group, (***) significance ($p < 0.05$) compared to all groups at given time point. Data expressed as mean ± SEM, $n = 6$. Scale bars: 100 μm.

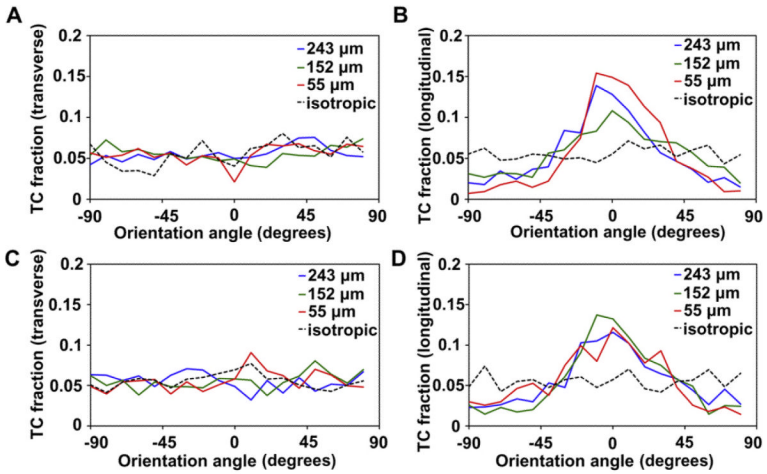

Fig. 5.

TC orientation within the scaffold network for the aligned (55 μm, 152 μm, 243 μm) and isotropic control scaffolds. A–D) Frequency plots of TC orientation angles: A) day 7 (transverse), B) day 7 (longitudinal), C) day 14 (transverse), and D) day 14 (longitudinal).

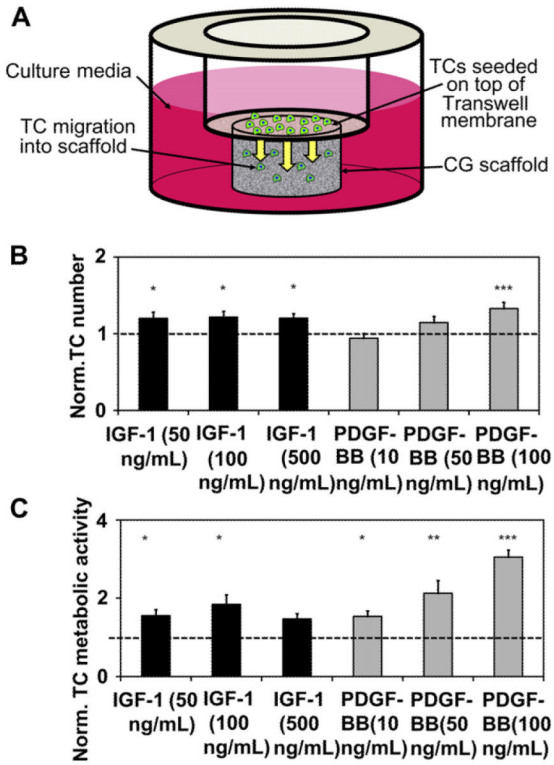

Fig. 6.

TC chemotaxis into aligned (243 μm pore size) CG scaffolds in response to PDGF-BB, IGF-1. A) Schematic of experimental set-up to study TC chemotaxis into the scaffold. B) Normalized TC number and C) metabolic activity of migrated cells in aligned CG scaffolds compared to non-supplemented control (dashed line). (*) significance ($p < 0.05$) compared to control, (**) significance ($p < 0.05$) compared to control and PDGF-BB (10 ng/mL), (***) significance ($p < 0.05$) compared to all other experimental groups. Data expressed as mean ± SEM, $n = 5$.

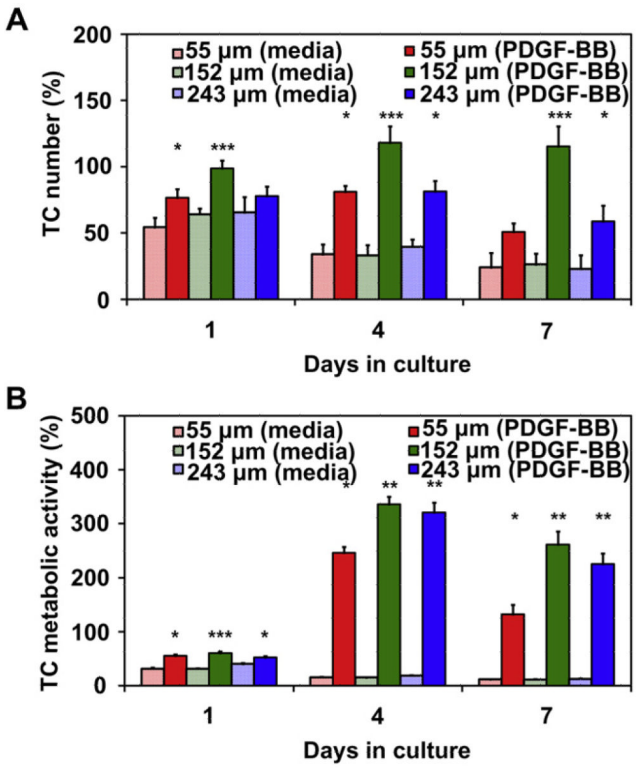

Fig. 7.

TC number and metabolic activity in aligned (55 μm, 152 μm, 243 μm) scaffolds supplemented with PDGF-BB. A) TC number and B) metabolic activity over 7 days in culture in aligned scaffolds supplemented with PDGF-BB (100 ng/mL). Solid bars represented supplemented media; patterned bars represented non-supplemented control. (*) significance ($p < 0.05$) compared to media control for same pore size at that time point, (**) significance ($p < 0.05$) compared to PDGF-BB supplemented 55 μm group at that time point, (***) significance ($p < 0.05$) compared to all other experimental groups at that time point. Data expressed as mean ± SEM, $n = 6$.

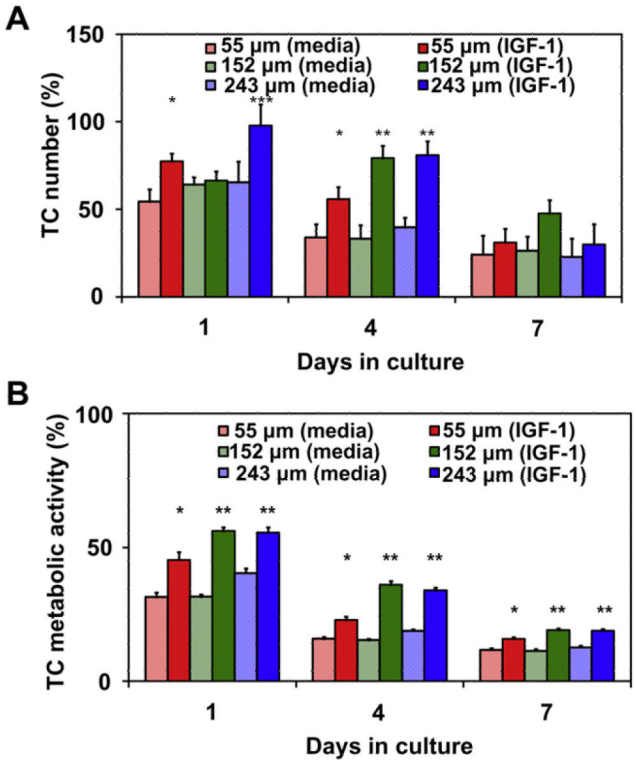

Fig. 8.

TC number and metabolic activity in aligned (55 μm, 152 μm, 243 μm) scaffolds supplemented with IGF-1. A) TC number and B) metabolic activity over 7 days in culture in aligned scaffolds supplemented with IGF-1 (100 ng/mL). Solid bars represented supplemented media; patterned bars represented non-supplemented control. (*) significance ($p < 0.05$) compared to media control for same pore size at that time point, (**) significance ($p < 0.05$) compared to IGF-1 supplemented 55 μm group at that time point, (***) significance ($p < 0.05$) compared to all other experimental groups at that time point. Data expressed as mean ± SEM, $n = 6$.

Table 1

Mean pore size from the transverse plane as well as the pore aspect ratios from the transverse and longitudinal planes for the three aligned CG scaffold variants created at distinct freezing temperatures (−10 °C, −40 °C, and −60 °C). Pore aspect ratios in the longitudinal plane are significantly (*$p < 0.0001$) greater than in the transverse plane for each freezing temperature, indicating that pores are elongated in the direction of the scaffold longitudinal axis. Data expressed as mean ± standard deviation, $n = 3$.

Freezing Temperature	Transverse pore size	Pore aspect ratio
−10 °C	242.7 ± 28.8 μm	Transverse: 1.19 ± 0.12
		Longitudinal: 1.57 ± 0.23*
−40 °C	152.4 ± 25.1 μm	Transverse: 1.17 ± 0.08
		Longitudinal: 1.63 ± 0.17*
−60 °C	55.3 ± 17.6 μm	Transverse: 1.07 ± 0.04
		Longitudinal: 1.41 ± 0.16*